JOURNAL OF AIRCRAFT
Vol. 30, No. 4, July–Aug. 1993

Wake Structure of a Helicopter Rotor in Forward Flight

G. Briassulis* and J. Andreopoulos†
City College of the City University of New York, New York, New York 10031

The wake of an idealized two-bladed helicopter rotor in forward flight has been experimentally investigated using hot-wire anemometry techniques. A model was designed, constructed, installed, and tested in a wind tunnel. Time-dependent measurements of three-dimensional velocity vectors were obtained for two pitch angles corresponding to a Reynolds number based on the rotor tip rotational velocity and blade chord of 8.2×10^4 and 6.2×10^4, respectively, at an advance ratio of 0.15. The results include time- and phase-averaged data of mean velocity components and turbulence intensities, as well as spectral analysis. Profiles of the streamwise component of the velocity vector have shown the existence of an Ω_z component of the vorticity vector. Analysis of the vertical and the transverse component of the velocity vector also revealed the existence of an Ω_x component of the vorticity vector at both edges of the wake. Large levels of turbulent kinetic energy were found almost everywhere in the wake. Turbulence intensity due to the presence of the counterclockwise rotating vortex reached the maximum values of 22.4 and 19% for pitch angle 10 and 6 deg, respectively. Spectral analysis of the velocity components revealed peaks of power spectral densities at frequencies two or four times higher than the blade passage frequency. This suggests a possible breakup of the vortex sheets roll-up or tip vortices due to large scale instabilities.

Nomenclature

A	=	rotor disk area = πR^2, m^2
A_1, A_2, A_3	=	hot-wire calibration constants
B_1, B_2, B_3	=	hot-wire calibration constants
b	=	number of blades
c	=	blade chord, m
c_s	=	speed of sound, m/s
C_T	=	rotor thrust coefficient, $T/\rho A(\omega R^2)$
D	=	rotor diameter, m
E	=	hot-wire voltage output, V
f	=	frequency, Hz
f_0	=	rotor frequency, Hz
h_1, h_2, h_3	=	hot-wire coefficient for pitch response
j	=	bin of the phase average routine
$j1(j)$	=	number of data points in the jth bin
k_1, k_2, k_3	=	hot-wire coefficient for yaw response
M_{tip}	=	blade tip Mach number = $\omega R/c_s$
N	=	population or data length
n	=	exponent in King's law
$\overline{q^2}$	=	turbulent kinetic energy, $\frac{1}{2}(\overline{u^2} + \overline{v^2} + \overline{w^2})$, m^2/s^2
S_{uu}	=	power spectral density of the $\tilde{u} + u$ fluctuation
S_{vv}	=	power spectral density of the $\tilde{v} + v$ fluctuation
S_{ww}	=	power spectral density of the $\tilde{w} + w$ fluctuation
T	=	thrust, N
$\bar{U}$	=	mean velocity in the x direction, m/s
U_0	=	tunnel freestream velocity, m/s
U_{eff}	=	effective cooling velocity, m/s
(U_N, U_T, U_B)	=	normal, tangential, and binormal component of the velocity vector in wire coordinates, m/s
(U, V, W)	=	velocity components in x, y, z directions in laboratory coordinates, m/s
u	=	turbulent part of the instantaneous velocity, m/s
$\tilde{u}$	=	periodic part of the instantaneous velocity, m/s
v_i	=	rotor-induced velocity, m/s
(X, Y, Z)	=	velocity components in probe coordinates
(x, y, z)	=	laboratory coordinates
(x_1, y_1, z_1)	=	probe coordinates
α	=	angle of attack, deg
$\Delta\theta$	=	bin size, deg
$\Delta\phi$	=	angle between two adjacent measurements, deg
θ	=	pitch angle, deg
λ	=	rotor inflow ratio = $(U_0 \sin\alpha + v_i)/\omega R$
μ	=	advance ratio = $U_0 \cos\alpha/\omega R$
ρ	=	density, kg/m^3
σ	=	rotor solidity = $bc/\pi R$
ϕ	=	azimuth, deg
$\phi(i)$	=	initial blade angle, deg
Ω_x, Ω_z	=	x and z components of the vorticity vector
ω	=	rotor speed, rad/s
$\langle\ \rangle$	=	ensemble average
$\tilde{}$	=	periodic part
$\bar{}$	=	time average

Presented as Paper 91-1753 at the AIAA 22nd Fluids Dynamics, Plasmadynamics, and Lasers Conference, Honolulu, HI, June 24–27, 1991; received July 17, 1991; revision received March 12, 1992; accepted for publication May 21, 1992.

*Graduate Student, Experimental Fluid Mechanics and Aerodynamics Lab, Department of Mechanical Engineering. Member AIAA.

†Professor, Experimental Fluid Mechanics and Aerodynamics Lab, Department of Mechanical Engineering. Member AIAA.

I. Introduction

A ROTOR in low speed forward flight operates in an unsteady and three-dimensional flow field. The wake of the rotor contains sprong vortices and vortex sheets.

When distributed vorticity encounters lifting surfaces, it induces strong temporal variations of the pressure distribution. Such disturbances often are due to vortex sheets which roll into vortices.

A better understanding of the instantaneous structure of the wake and a more detailed insight into the involved phenomena can provide a more precise determination of the effects of these phenomena on the vibration of the rotor blades and on the noise production. The control of sound generation and dynamic response of the structures require understanding of the fundamental phenomena involved. In addition, the lift and drag characteristics of the rotor blades are substantially

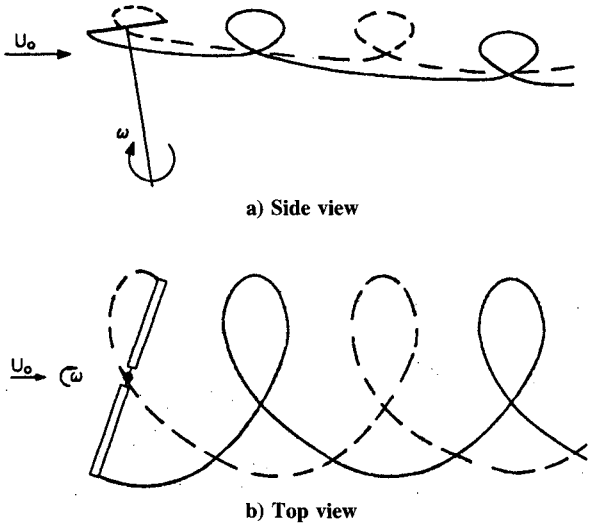

Fig. 1 Flow configuration in the wake of two-bladed helicopter rotor.

affected by the near wake, while the performance of the tail-rotor/tail-boom control surfaces is significantly altered by the far wake.

The objectives of the present experimental work are to improve our physical understanding of rotor wake flows in the presence of a cross stream by looking closer at the vortex dynamics of the flow, particularly in the far-wake region, and to obtain a reliable and comprehensible turbulence data which will be used for testing and improving turbulence modeling and calculation methods for these types of flows. Lack of reliable experimental turbulence data, which are needed for validation of such methods, considerably hampers their development towards better predicting capabilities of rotor flows. Figures 1a and 1b show a schematic of the flow in the rotor wake of a two-bladed helicopter rotor in forward flight.

In the present work, an idealized flow case has been simulated in the absence of any compressibility effects, aeroelastic, or airframe interactions. This article presents selective results from the experiment.

II. Previous Work

Over the years, many experimental and theoretical attempts were made to reveal the behavior of rotating blades.

One of the major characteristics of the rotor wake flow, as it has been demonstrated by Heyson[1] and Heyson and Katzoff,[2] is the roll-up of the vortex sheet to form a pattern of two vortices similar to the trailing edge vortices of a low-aspect ratio fixed wing.

Tangler et al.[3] have shown that tip vortices interact strongly with each other so that the wake first contracts and then expands. It is also claimed that the vortices break down in a way that is similar to the vortex breakdown occurring over delta wings.

Extensive analytic and experimental investigations related to applied problems of helicopter performance and wake geometry characteristics have been conducted by Landgrebe and his associates.[4-6]

Several researchers[7-10] conducted blade/vortex interaction (BVI) experiments to obtain the aerodynamic performance of the airfoil and to explain some of the phenomena present in rotor wake flows, such as vortex structure and blade slap.

Since experimental work was limited to hovering blades, Brand et al.[11] conducted an experiment simulating the forward flight of a rotor with the presence of an airframe model. Correlating with velocity data indicated that velocities induced by the vortex can be as large as 20% of the blade tip speed. In conclusion, they found that the motion of the tip vortex is strongly affected by the presence of other nearby vortices from other blades or from previous revolutions.

Similar experimental work was carried out by Liou et al.[12-14] to investigate the velocity field of a lifting rotor in low speed forward flight. They found that the distribution of the time-averaged velocity normal to the tip path plane is not symmetrical with respect to the longitudinal axis. The strongest downflow was occurring around 70 and 270 deg. Their measurements, however, were confined to the near vicinity of the blades and did not include any measurements in the downstream region of the wake.

Nsi Mba et al.[15] acquired data near the blades which led them to determine the distribution of circulation along the blade span. They found that for a hovering rotor with symmetrical NACA 0012 airfoils, the maximum circulation (Γ) was located at the radial station $r/R = 0.80$. It was also shown that the presence of sign-inverted velocities at the low blade radius r/R induces negative values of Γ near the root.

Cheeseman and Haddow[16] investigated the downwash effect just beneath a specialized lifting rotor up to $0.3R$ downstream. They reported that the roll-up of the vortex sheet at the tip takes place rapidly and is completed within 5-deg azimuth angle after the blade passage.

Leishman and Bi,[17] using a miniature pressure probe, conducted an experiment to investigate the wake of the rotor and fuselage in forward flight as well as the effects of the rotor flowfield on the body.

In addition to experiments, extensive numerical methods have been developed to theoretically analyze the helicopter rotor flow. Recently, Chen and McCroskey[18] presented their work simulating a helicopter with blade rotor flow. Even though approximations are associated with any numerical method, the authors were able to obtain good agreement with experimental data in either hover or forward flight. In their work, the experimental data used for comparison was that of Caradonna et al.[19] They concluded that near-wake effects can be captured without wake modeling. A similar theoretical study was carried out by Berry.[20] In his work, he also attempted to simulate the geometry and effects of a helicopter rotor wake in forward flight.

Flow visualization has been found to be a very powerful technique in revealing several key characteristics of the physics of this very complicated wake flow. Light et al.[21] used the wide-field shadowgraph method for a four-bladed rotor. They report that tip vortices are visible for low advance ratios up to 0.175, provided that the rotor thrust is high enough. Tangler[22] and Tangler et al.,[3] experimenting with a high speed rotor, showed the bow shocks created by the blades as well as the location of the vortical structures. They also reported that the blade vortex intersections can be found in all four quadrants, but not all of them can be observed by the upper surface. Jenks et al.[23] and Lehman[24] investigate the flowfield in water tanks for various pitch angles and angular velocities. Jenks et al.[23] show the tip vortices at different azimuth angles as well as the vortex sheet roll-up. Lehman[24] concentrates more on the overall structure of the wake such as wake boundaries and effects of different rotor configuration on the wake. More recently, Leigthy et al.[25] demonstrated the use of a flow-synchronized strobed laser light sheet to visualize the wake of a four-bladed rotor tilted 5.8 deg. Their technique was capable of following consecutive blade-tip vortices in space. Interpretation of their results is still to come.

The approach adopted in the present investigation was that of a basic research project. The real helicopter wake is indeed an extremely complicated flow. The flow interference with the airframe below the rotor, e.g., blade flapping and aeroelastic interactions and blade tip compressibility effects, are phenomena which considerably change the vortex dynamics of the wake, and therefore, tend to make our physical understanding more difficult. By looking into the flow in the absence of these additional effects, the potential of better understanding the vortex dynamics of the wake and eventually being able to control it, is much greater than directly facing a multiparameter problem. Therefore, the present work should be

considered as an idealized situation of the real flow, and not as an attempt to fully simulate the actual helicopter wake.

III. Experimental Set-Up

The experiments were performed at the CCNY large-scale wind tunnel. The tunnel has a 20-bhp capacity ac motor which is frequency controlled and can drive 1133 m^3/min (40,000 ft^3/min) of air at a maximum freestream velocity of approximately 11 m/s. At the inlet, the flow passes through the 3.66 × 3.66 m (12 × 12 ft) cross-sectional area which contains a honeycomb and five mesh screens. The cross-sectional area is contracted to 1.22 × 1.22 m (4 × 4 ft) in the last section, thus giving a 9:1 reduction in area. The test section is 6.1-m (20-ft) long, ending at the beginning of the fan/motor section. The present model consisted of 1) two NACA 0015 blades, 2) shaft 1.9 cm ($\frac{3}{4}$ in.) in diameter, and 3) rotor hub. The blades were rigidly attached on the rotor hub. This assembly, shaft, rotor hub, and blades, was statically and dynamically balanced in order to minimize vibrations, and therefore, minimizing blade deflection due to rotation.

Two experiments were carried out, one at pitch angle 6 deg and one at pitch angle 10 deg. For both experiments, the advance ratio μ was kept constant, and equal to 0.15. This was accomplished by adjusting the tunnel speed and/or the angular velocity of the rotor.

For 6-deg pitch, the tunnel was operating at $U_0 = 8.8$ m/s while the angular velocity of the blades was 1200 rpm. For 10-deg pitch, the tunnel was operating at $U_0 = 6.6$ m/s and the angular velocity of the blades was 900 rpm. These values were chosen from a range of wind-tunnel velocities and angular velocities of the blades to be the ones with minimum flow-induced vibrations. A summary of the rotor characteristics and the flow parameters is given in Table 1.

A brushless electric motor model KH 720 made by Compumotor was used to drive the wooden blades, which were a NACA 0015 airfoil section of 0.942-m diam, at various angular speeds up to 2500 rpm. The advantage of this motor was that a single revolution was resolved by 25,000 individual steps. Using the built-in indexer of the drive, the motor can be rotated to a precise position and at a constant angular velocity during each revolution of the blades. The accuracy of the angular velocity of this type of motor was ±0.00628 (rad/s). The drive was able to communicate through a controller card with an IBM XT computer to monitor and control the angular position of the rotor assembly. The XT was communicating through an RS232 interface with the IBM AT so that data acquisition and location of the blades were recorded simultaneously.

To achieve variable pitch angle of the rotor, a mechanism was designed and built to hold the motor and tilt the whole assembly of shaft, hub, and blades.[26] The motor and this mechanism were mounted on the floor below the working section outside the wind tunnel (as shown in Fig. 2a).

The blades were placed inside the wind tunnel so that the hub is 15.24-cm (6-in.) below the middle horizontal plane of the working section, to allow for wake flow development with minimum interference by the tunnel ceiling, since the induced flowfield displaces the flow upwards. It is known[16,17,23] that the rotor wake in presence of a cross stream, with larger momentum than that of the induced flow, contracts considerably as it develops downstream. This has been also confirmed by the present results. If the wake was considered as a solid body without fluid entrainment, its blockage could be 4.6% of the tunnel cross section. No corrections were made to the data because this blockage ratio is considered insignificant in causing any tunnel wall interference. In addition, since the thrust of the present rotor is very small, the circulation or strength of any of the vortices in the wake should be also small, and therefore, the effect of the image-vortices with respect to the tunnel wall is expected to be very weak.

The model was inverted and installed in the wind tunnel with the rotating shaft placed upstream of the rotor. This configuration was more preferable than placing the shaft downstream in terms of additional shaft-wake effects. Thus, if the shaft was placed downstream of the rotor, then the shaft itself would be longer and interfere directly with the rotor wake. In the present configuration, shaft-wake effects would be small by the time they reached the location of measurements in the rotor wake because they would decay with downstream distance.

Data was acquired at five locations downstream for the center plane and two locations for each of the two off-center planes for both pitch angles. At each location, profiles were taken every 10 mm, except at tip level when they were taken every 2 mm for a total of 140 stations for each pitch angle. A detailed grid of the measurement area is shown in Fig. 2b. It contains locations in the near field as well as in the far field, where to the best of our knowledge, no previous measurements have been attempted. At each station, 10,800 measurements were acquired at a sampling frequency of 694 Hz for pitch angle of 6 deg and 926 Hz for pitch angle of 10 deg, recording over 160 revolutions of the blades. The above gave a sampling resolution of 5.83 deg of azimuth angle for pitch

Table 1 Flow parameters and rotor characteristics

Rotor characteristics	Flow parameters
Number of blades	2
Rotor radius	0.471 m
Blade chord	0.04445 m
ω	900 and 1200 rpm
Rotor solidity	0.0604
Aspect ratio	10.6
Blade twist	0 deg
Aerofoil section	NACA 0015

Rotor pitch angle	6 deg	10 deg
ωR	29.6 m/s	22.2 m/s
M_{tip}	0.085	0.064
Cr (estimated)	0.0055516	0.00967
T (estimated)	3.38 N	3.315 N
μ	0.15	0.15
Re_c	8.2×10^4	6.2×10^4

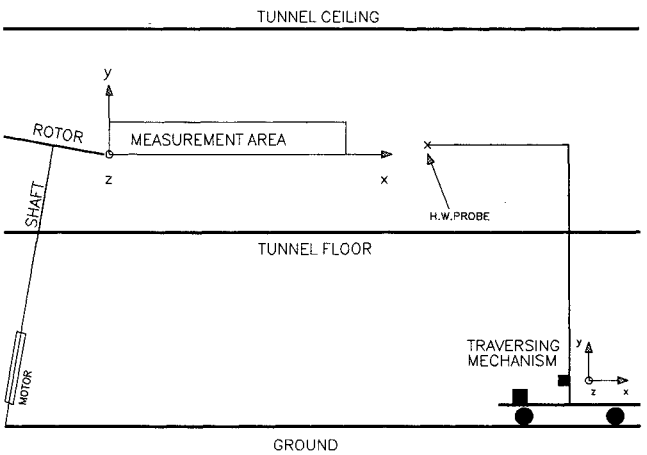

Fig. 2a Experimental set-up.

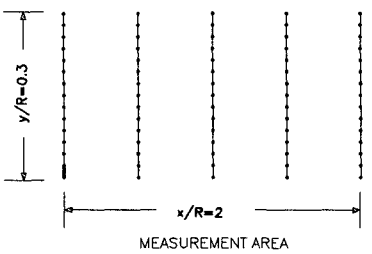

Fig. 2b Measurement locations.

angle 10 deg, and 10.37 deg of azimuth angle for pitch angle 6 deg. The reference azimuth angle, $\phi = 0$ deg, was taken when the blades were perpendicular to the freestream vector.

A 5-μm homemade triple hot wire probe was used to simultaneously measure the three velocity components as a function of time.[30]

The effective cooling velocity of each of the three wires in the King's law, $E^2 = A + BU_{\text{eff}}^n$ has been expressed according to the formula

$$U_{\text{eff}} = (U_N^2 + k^2 U_T^2 + h^2 U_B^2)^{1/2}$$

as it has been proposed by Jorgensen.[31] The coefficients k^2 and h^2 are determined by yaw and pitch calibrations.

The basic feature of the present probe is that its wires are parallel to the axis of an orthogonal coordinate system (probe coordinate system) so that the tangential component of one wire is normal for another, and binormal for the third. If the instantaneous velocity vector has components X, Y, Z parallel to the respective probe coordinates x_1, y_1, z_1 (see Fig. 3) then the effective cooling velocity for each wire is given by

$$[(E_1^2 - A_1)/B_1]^{2/n1} = U_{\text{eff}_1}^2 = k_1^2 X^2 + Y^2 + h_1^2 Z^2$$

$$[(E_2^2 - A_2)/B_2]^{2/n2} = U_{\text{eff}_2}^2 = h_2^2 X^2 + k_2^2 Y^2 + Z^2$$

$$[(E_3^2 - A_3)/B_3]^{2/n3} = U_{\text{eff}_3}^2 = X^2 + h_3^2 Y^2 + k_3^2 Z^2$$

The above system of equations is linear with respect to X^2, Y^2, Z^2, and the instantaneous velocity components can be obtained in probe coordinates by matrix inversion shown below:

$$\begin{bmatrix} X^3 \\ Y^2 \\ Z^2 \end{bmatrix} = D^{-1} \begin{bmatrix} U_{\text{eff}_1}^2 \\ U_{\text{eff}_2}^2 \\ U_{\text{eff}_3}^2 \end{bmatrix}$$

where D is defined as

$$D = \begin{bmatrix} k_1^2 & 1 & h_1^2 \\ h_2^2 & k_2^2 & 1 \\ 1 & h_3^2 & k_3^2 \end{bmatrix}$$

The instantaneous velocity components in the laboratory coordinates can be obtained through a further coordinate transformation matrix N from the relation

$$\begin{bmatrix} U \\ V \\ W \end{bmatrix} = [N] \begin{bmatrix} X \\ Y \\ Z \end{bmatrix}$$

It should be pointed out that the coefficients k_i and h_i are not necessarily the same for all wires. For instance, the average value for h_1^2 was found to be 1.46, for h_2^2 was 1.344, and for h_3^2 was 1.014. Also, the average value for k_1^2 was 0.02, for k_2^2 was 0.0176, and for k_3^2 was 0.015. The results, particularly the V velocity component, are very sensitive to the values of k_2 and h_2 which are determined by a tedious yaw and pitch calibration of the probe.

The measurements of Cheeseman and Haddow,[16] for example, have been obtained without a proper calibration of the probe, and therefore, their validity is doubtful because of lack of knowledge of the behavior of the yaw and pitch response of the wires.

The signal output of the triple hot wire was free of spikes and the noise level was below 2 mV. The near-wake flow is of high turbulence intensity without any flow reversals. Brand et al.[11] reported that flow reversals take place very near the blades where the flow may be occasionally separated. Therefore, careful use of hot wire techniques in regions without flow reversals is permissible. It should be mentioned that, in general, this probe can recover the instantaneous velocity vector if this lies within the acceptance "cone." This cone is geometrically defined by the position of the sensing wires. However, the accuracy of the measurements improve substantially when the pitch and yaw angle of the velocity vector is less than ± 30 deg.[27,30,32,33] This indicates that sudden change of the flow due to vortex passage can be depicted quite well by the probe.

The triple hot wire was driven by three DANTEC constant temperature anemometers type 56C17. The three signals were digitized by a DASH-20 Metrabyte Analog to Digital Converter which has a 100 kHz maximum sampling rate and 12 bit/word resolution. A Metrabyte Sample and Hold unit, model SSH4, was also used for simultaneous sampling of all channels. All hot-wire signals, as well as the Pitot tube pressure transducer output were monitored by two digital oscilloscopes type IWATSU OS-6612. The hot-wire probe was mounted on the traversing mechanism shown in Fig. 2a. The traversing mechanism was computer-controlled and could provide, by using stepper motors, three translational motions along the x, y, z directions and two rotational motions about the y and z axes for pitch and yaw orientation of the probe. In order to minimize interference effects in the flowfield, the arm of the traversing mechanism was 1-m long (20 diam of the mechanism's vertical rod).

Error analysis indicated a 6% uncertainty in the measurements of mean velocity components and 8% in the measurements of turbulent kinetic energy. These values include errors due to discretization, resolution, calibration, and those caused by the high turbulence intensity (see Ref. 28).

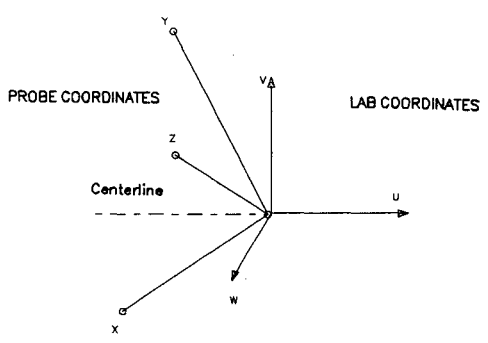

Fig. 3 Probe and lab coordinates.

IV. Data Reduction

For a time-dependent flow, it is useful to decompose the dependent variable into three parts. Namely, the velocity field response to a perturbation such as a helicopter rotor can be interpreted as

$$U(x, t) = \bar{U}(x) + \tilde{u}(x\, t) + u(x, t)$$

The three components of the instantaneous velocity are 1) the time-averaged or mean, 2) the periodic or deterministic, and 3) the turbulent part of the velocity field.

The time-averaged velocity component can be expressed as

$$\bar{U}(x) = \lim_{M\to\infty} \frac{1}{M} \sum_{m=0}^{M-1} u(x, t_0 + m\Delta t)$$

The time-average of a fluctuating quantity removes both background turbulence and periodic contribution.

The ensemble average or phase-average of the longitudinal velocity component is defined as

$$\langle U \rangle = \bar{U}(x) + \tilde{u}(x, t) = \lim_{N\to\infty} \frac{1}{N} \sum_{n=0}^{N-1} u(x, t + n\tau)$$

where $M\Delta t \gg \tau$, and τ is the period of the cycle.

The average over a large ensemble of points, with respect to the reference, effectively filters out background turbulence. For this matter, any turbulent quantity measured in the wake of the rotor can be averaged in bins of prescribed width in order to obtain averages with respect to the azimuth angles of the rotating blades. The average in each bin can be expressed as

$$U(j) = \left[\frac{\sum_{n=1}^{N(j)} U(j, n)}{N(j)} \right]$$

with

$$j = \text{integer} \left\{ \frac{[\phi(n) + (n - 1)\Delta\phi]}{\Delta\theta} \right\}$$

where $\Delta\theta$ is the bin width, $\Delta\phi = \omega\Delta t$ is the angle between two consecutive measurements, $N(j)$ is the number of data points in the jth bin, (360 deg/$\Delta\theta$) is the maximum number of bins, and $\phi(n)$ is the initial blade angle when data acquisition was begun.

Similar operations were used to deduce other quantities such as turbulent kinetic energy and shear stresses.

Spectral analysis of the signals was carried out by using Fast Fourier Transforms.

V. Results

The results of this investigation include conventional statistical time-averages, phase-averages of three velocity components, turbulent kinetic energy and shear stresses, probability density function of the three velocity components, as well as spectral analysis of the signals. Only a selection of the results will be presented here, while details of the work and more data can be found in the thesis by Briassulis.[26] All velocity data have been normalized by the freestream velocity U_0 of the incoming flow.

Figure 4 shows a typical distribution of the mean U velocity profile in the wake for pitch angle 6 deg. Several profiles at $z/R = 0$ indicate typical wake or shear layer type of behavior with substantial gradients which suggest the existence of strong vorticity in the field. The profiles at x/R = 1.0, 1.5, and 2 show a small positive velocity gradient $\partial U/\partial y$, which results in higher velocity at large y/R positions than at $y/R = 0$. This is most probably due to the strength of the induced velocity which is diminishing with increasing y/R distance. That is, a rotor with higher thrust is expected to produce more intense vortical structures that would affect the wake flow further downstream. Similar behavior can be depicted in the case of pitch angle 10 deg for two different downstream positions at $z/R = -1.0$, shown in Fig. 5. Both profiles show a small velocity deficit which is typical of a wake flow.

Profiles of turbulent kinetic energy $\overline{q^2} = \frac{1}{2}(\overline{u^2} + \overline{v^2} + \overline{w^2})$ are shown in Figs. 6 and 7 for pitch angles 6 and 10 deg, respectively. It is interesting to see that the wake is fully turbulent and in several locations the corresponding turbulence intensity is extremely high (of the order of 25%). Peaks in the distributions of $\overline{q^2}$ are evident in the near field, whereas, at far downstream stations, the distribution of $\overline{q^2}$ is more uniform due to gradient diffusion type of turbulent kinetic energy transport. At higher pitch angles, $\overline{q^2}$ is increased particularly at locations close to the rotor blades. An approximate sense of the turbulent wake boundaries can be extracted from Figs. 6 and 7. It can be seen from Fig. 6 that the far wake is contracting. At $x/R = 0$ the turbulent boundary can be found at $y/R = 0.25$, and at $x/R = 2.0$ at $y/R = 0.23$ (9% contraction). For pitch angle 10 deg (Fig. 7) the wake is much more turbulent. Similar conclusions can be drawn from Fig. 7. At $x/R = 0$ the turbulent flow boundary can be found at $y/R = 0.38$, and at $x/R = 2.0$ at $y/R = 0.29$ (25% contraction). That is, tip vortices are stronger for higher pitch angles. They interact and attract each other, and therefore, the turbulent wake will contract more for higher pitch angles.

Figure 8 shows the phase-averaged distribution of the three velocity components for pitch angle 10 deg at $z/R = -1.0$, $x/R = 0$, and $y/R = 0.255$. All distributions indicate a certain periodicity with some phase lag between them. $\langle V \rangle$ and $\langle W \rangle$

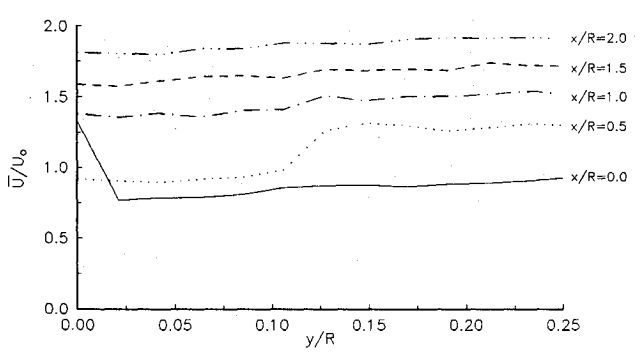

Fig. 4 Mean velocity profiles for pitch angle 6 deg, $z/R = 0$ for various downstream positions. Velocity axes for $x/R = 0.50$, 1.0, 1.5, and 2 are shifted 0.25, 0.50, 0.75, and 1.0 units, respectively. Lines are drawn through the data points for visual aid.

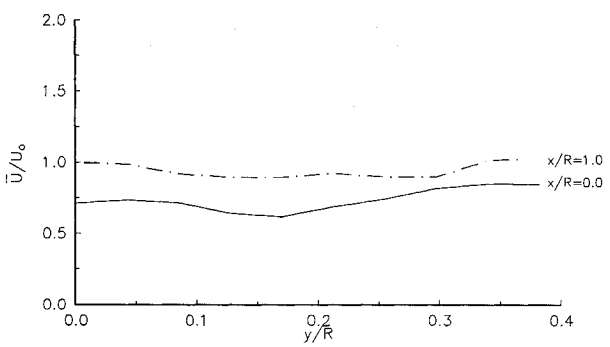

Fig. 5 Mean velocity profiles for pitch angle 10 deg, $z/R = -1.0$ for two downstream positions. The $x/R = 1.0$ axis is shifted 0.25 units.

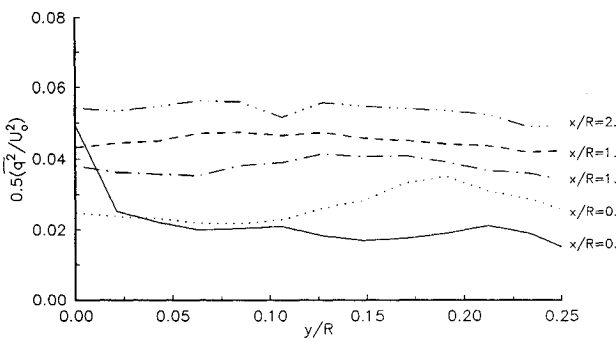

Fig. 6 Profiles of turbulent kinetic energy for pitch angle 6 deg, $z/R = 0$ for various downstream positions. The axes $x/R = 0.50$, 1.0, 1.5, and 2 are shifted 0.25, 0.50, 0.75, and 1.0 units, respectively.

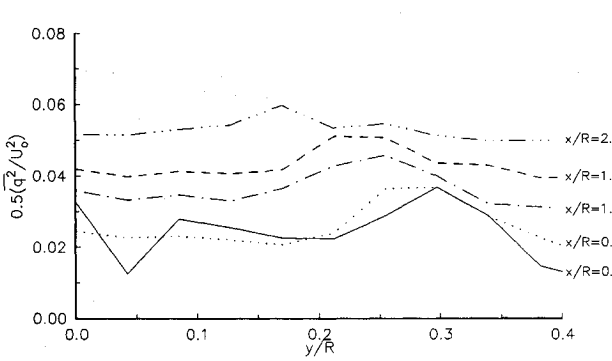

Fig. 7 Profiles of turbulent kinetic energy for pitch angle 10 deg, $z/R = 0$ for various downstream positions. The axes $x/R = 0.50$, 1.0, 1.5, and 2 are shifted 0.25, 0.50, 0.75, and 1.0 units, respectively.

components are zero crossing practically at the same phase, indicating the existence of strong streamwise vorticity at this particular location.

Figure 9 shows the phase-averaged turbulent kinetic energy at the above-mentioned position and two other positions ($y/R = 0.106$ and $y/R = 0.0$). Turbulence intensities at $y/R = 0.255$ shows that at the peak, which takes place at a phase angle $\phi = 220$ deg, the turbulence intensity $\sqrt{\overline{q^2(\phi)}}/\langle U(\phi)\rangle$ ($\langle U(\phi)\rangle$ can be found in Fig. 8) corresponds to a value of 30%, while the minimum value in the whole cycle appears to be about 20%. This indicates that there is no position in the cycle with low turbulent intensity. From Fig. 9, we can get a sense of the distribution of turbulence in the wake. Blade passages can be seen at $y/R = 0.106$ for $\phi = 112$ deg and $\phi = 292$ deg which correspond to a phase lag of 22 deg.

The spatial evolution of the phase-average $\overline{q^2}$ is shown in Figs. 10 and 11, where $\overline{q^2}$ is plotted for several typical phase values at downstream locations. Two peaks are present at almost all phases at $x/R = 0$, most probably due to vortex passage (Fig. 10), while turbulent diffusion evened out any nonuniformities of $\overline{q^2}$ at $x/R = 1.0$ (Fig. 11).

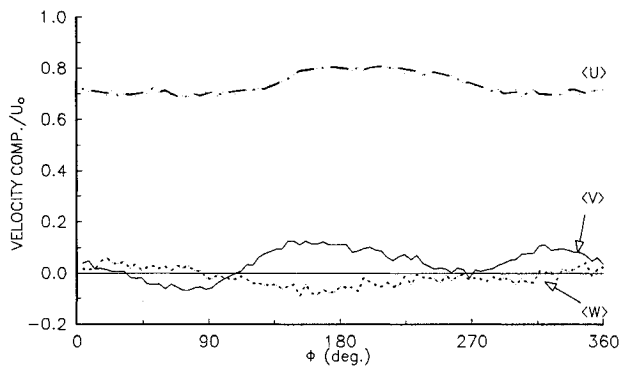

Fig. 8 Phase-averaged distribution for pitch angle 10 deg, $z/R = -1.0$, $x/R = 0$, $y/R = 0.255$ for three velocity components.

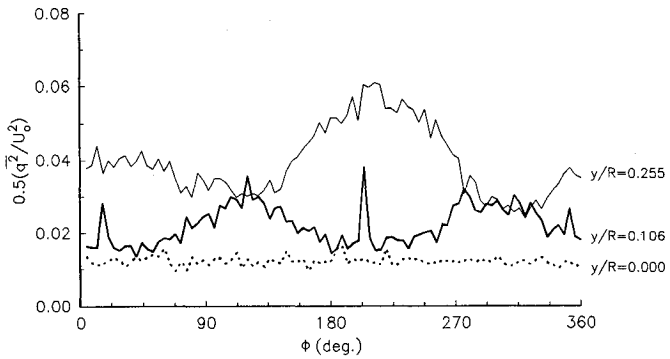

Fig. 9 Turbulent kinetic energy profile for pitch angle 10 deg, $z/R = -1.0$, $x/R = 0$, for three different heights.

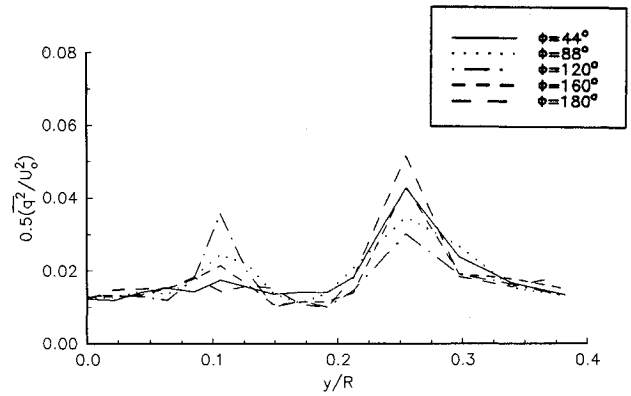

Fig. 10 Profiles of turbulent kinetic energy for pitch angle 10 deg, $z/R = -1.0$, $x/R = 0$ for various azimuth values.

Typical results of the spectral analysis are presented in Fig. 12. Power spectral density of the three velocity components u, v, and w at $z/R = -1.0$, $x/R = 0$, and $y/R = 0.255$ are shown in Figs. 12a, b, and c, respectively, for pitch angle 10 deg. The fundamental frequency f_0 is the fundamental frequency of the rotor 15 Hz. Peaks of spectral densities can be observed almost at all harmonics up to the 8th. Since the rotor consists of two blades, the blade passage frequency is $2f_0$. It is interesting to observe that the amplitude of the v component spectral density is larger than in the other components, indicating that the v component is more receptive at this frequency, $2f_0$, rather than at the fundamental f_0. Similar behavior has been found in the von Kármán vortex street behind a circular cylinder where the v component is used to detect periodicities in the wake. The most probable physical phenomenon associated with the appearance of higher harmonics seems to be the splitting or breakup of the tip vortex or vortex sheet into two or more vortical structures. Amalgamation or

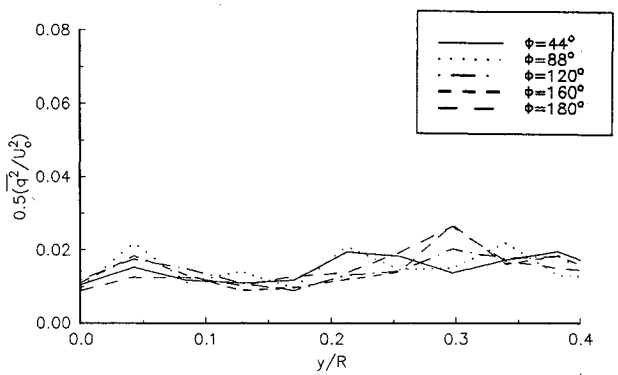

Fig. 11 Profiles of turbulent kinetic energy for pitch angle 10 deg, $z/R = -1.0$, $x/R = 1.0$ for various azimuth values.

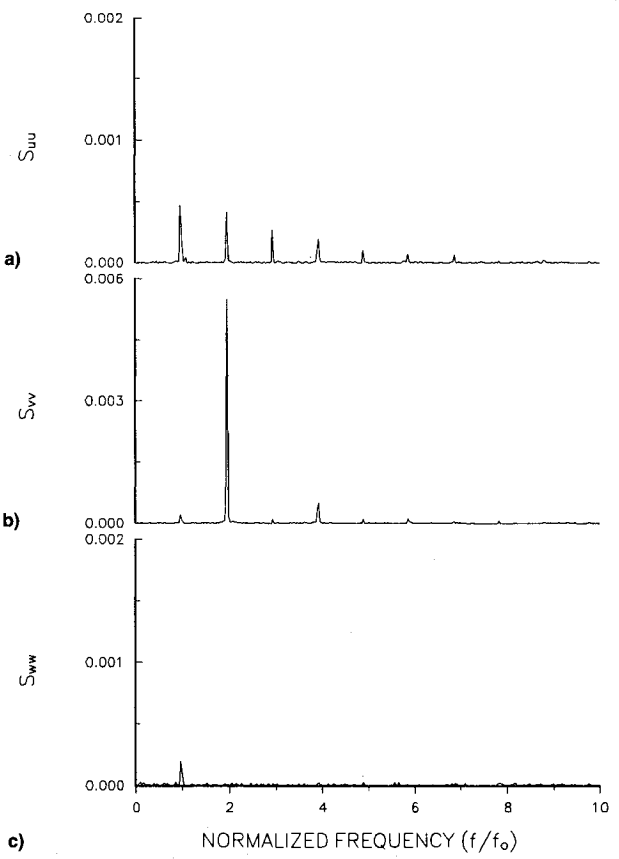

Fig. 12 Power spectral density (S) of u, v, and w component, respectively, at $x/R = 0$, $z/R = -1.0$, $y/R = 0.255$ for pitch angle 10 deg. The frequency domain (f) is normalized by the rotor frequency (f_0).

coalescence of vortices can be ruled out because it results in frequency halving rather than frequency doubling. The frequency of appearance of the tip vortices is that of the blade passage frequency. In addition, the higher harmonics peaks are only in the u and v components, suggesting that these structures carry mainly Ω_z vorticity. Brand et al.[11] pointed out that large induced velocity effects of the vortices on each other exist in the wake, and that the interaction is quite strong. The present results indicate that these highly distorted vortex sheets and tip vortices split or breakup due to strong mutual interactions which cause large instabilities.

VI. Conclusions and Final Discussion

A study of a helicopter rotor in forward flight has been attempted in a wind tunnel. The experiments revealed several key characteristics of the flowfield in the rotor wake region at a constant advance ratio $\mu = 0.15$ and two pitch angles 6 and 10 deg.

Mean values of velocities and turbulent kinetic energy, as well as phase-averaged distribution and probability density functions (not shown here), were computed and used to interpret the results. Consistent results were obtained for both pitch angles.

Profiles of turbulent kinetic energy, presented for the first time, indicated that the wake of the rotor is highly turbulent and that its turbuence is increasing with pitch angle. It is therefore obvious that any attempt to compute the complex wake flow of a rotor blade should include a satisfactory modeling of turbulence. Inviscid flow calculations have a rather limited potential to adequately predict these flows.

The measurements indicated the existence of substantial vorticity in the flowfield which is associated with the vortex sheets shed off the blades and/or the vortex emanating from the blade tip. This vortical system is rather difficult to visualize and its vortex lines have different orientations at different locations inside the flowfield. It is also very difficult to attribute any vorticity measured in the flow to the tip vortex and not to the vortex sheet or vice versa. However, it is reasonable to assume that any vorticity found in the lower or upper edge of the wake is due to the tip vortices, and that any vorticity found in the inner flowfield is associated with the vortex sheet.

Vortices emanating from the two blade tips were found in every plane tested for both pitch angles. Analysis of the data have shown the presence of a clockwise rotating vortex at the lower edge of the wake ($y/R = 0$) and the presence of a counterclockwise rotating vortex at the upper edge of the wake ($y/R = 0.2$ for pitch angle 6 deg, and $y/R = 0.32$ for pitch angle 10 deg) in most of the planes tested. More specifically, the effects of the Ω_z component of the vorticity vector were found through analysis of the streamwise component of the velocity vector for the center plane and for the plane $z/R = -1.0$. The velocity distribution at the plane $z/R = -0.50$ was reasonably constant, and therefore, the Ω_z vorticity was negligible at this plane.

Furthermore, Ω_x component of the vorticity vector was found to be present inside the rotor wake. Analysis of the vertical and the transverse component of the velocity vector had indicated the presence of a clockwise rotating vortex at the lower edge of the wake. A counterclockwise rotating vortex was found at the upper edge of the wake ($y/R \approx 0.2$ for pitch angle 6 deg, and $y/R \approx 0.32$ for pitch angle 10 deg). The trace of the vortex sheet between the two downstream stations was found to have an upward motion. A 40% increase in the height location of the vortex sheet was evident in every region where it was detectable.

The presence of the counterclockwise rotating vortex was associated with high values of turbulent kinetic energy.

At the location of the counterclockwise rotating vortex, the turbulence intensity was 22.4% for pitch angle 10 deg and $z/R = -1.0$. At the next downstream station ($\frac{1}{2}$ diameter away) the turbulence intensity was 14.1%. In contrast, for pitch angle 6 deg and $z/R = -1.0$ the turbulence intensity was 19%, and $\frac{1}{2}$ diameter downstream was 16.7%.

Phase-averaged results and spectral analysis provided some more insight of the structure of the wake. The v component is more receptive to blade passages than the w component. Peaks at higher harmonics were also found in the spectra of the u and v components suggesting a split or breakup of the vortex sheet or tip vortices. Direct blade vortex interaction seems not to be responsible for this effect since the wake of each blade is washed downstream away from the blade plane by the cross stream before the following blade interacts with it. The reason for this behavior is the large pitch angle of the rotor, which in conjunction with the advance ratio, does not allow a direct interaction between blade and vortex or vortex sheet. However, mutual interaction between the two tip vortices and/or vortex sheets may cause instabilities which can lead to a breakup of the vortices or vortex sheets. Several authors[11,29] have indicated a possible "secondary vortex generation" mechanism. The present results confirm this observation. However, peaks of spectra were also found at higher harmonics. This suggests that further splitting or breakup of the vortices takes place. Eventually, this mechanism leads to the appearance of more vortical structures rather than vortices which are responsible for the high turbulence intensities found in the wake.

References

[1]Heyson, H. H., "Preliminary Results from Flow-Field Measurements Around Single and Tandem Rotors in the Langley Full Scale Tunnel," NACA TN-3242, 1954.

[2]Heyson, H. H., and Katzoff, S., "Induced Velocities Near a Lifting Rotor with Nonuniform Disk Loading," NACA TR-1319, 1957.

[3]Tangler, J. L., Wohlfeld, R. M., and Miley, S. J., "Investigation of Vortex Stability, Tip Shapes, Compressibility, and Noise for Hovering Model Rotors," NASA CR-2305, Sept. 1973.

[4]Landgrebe, A. J., "The Wake Geometry of a Hovering Helicopter Rotor and Its Influence on Rotor Performance," *Journal of the American Helicopter Society*, Vol. 17, No. 4, 1972, pp. 3–15.

[5]Landgrebe, A. J., Taylor, R. B., Egolf, T. A., and Bennett, J. C., "Helicopter Airflow and Wake Characteristics for Low Speed and Hovering Flight," *Journal of the American Helicopter Society*, Vol. 27, No. 4, 1982, pp. 74–83.

[6]Landgrebe, A. J., and Bellinger, E. D., "An Investigation of the Quantitative Applicability of Model Helicopter Rotor Wake Patterns Obtained from a Water Tunnel," United Aircraft Research Lab. K910917-23, Dec. 1971.

[7]Hubbard, E. J., Jr., and Leighton, P. K., "Comparison of Model Helicopter Rotor Primary and Secondary Blade/Vortex Interaction Blade Slap," *Journal of Aircraft*, Vol. 20, No. 5, 1989, p. 346.

[8]Straus, J., Renzoni, P., and Mayle, E. R., "Airfoil Pressure Measurements During a Blade-Vortex Interaction and a Comparison Theory," AIAA 26th Aerospace Sciences Meeting, AIAA Paper 88-0669, Reno, NV, Jan. 1988.

[9]Caradonna, F. X., Lautenschlager, L. J., and Silva, J. M., "An Experimental Study of Rotor-Vortex Interactions," AIAA 26th Aerospace Sciences Meeting, AIAA Paper 88-0045, Reno, NV, Jan. 1988.

[10]Poling, R. D., Wilder, C. M., and Telionis, P. D., "Two-Dimensional Interaction of Vortices with a Blade," AIAA 26th Aerospace Sciences Meeting, AIAA Paper 88-0044, Reno, NV, Jan. 1988.

[11]Brand, A., Komerath, N., and McMahon, H., "Results from Laser Sheet Visualization of a Periodic Rotor Wake," *Journal of Aircraft*, Vol. 26, No. 5, 1989, p. 438.

[12]Liou, G. S., Komerath, M. N., and McMahon, M. H., "The Velocity Field of a Lifting Rotor in Low Speed Forward Flight," AIAA 26th Aerospace Sciences Meeting, AIAA Paper 88-0666, Reno, NV, Jan. 1988.

[13]Liou, G. S., Komerath, M. N., and McMahon, M. H., "Velocity Field of a Cylinder in the Wake of a Rotor in Forward Flight," *Journal of Aircraft*, Vol. 27, No. 9, 1990, p. 804.

[14]Liou, G. S., Komerath, M. N., and McMahon, M. H., "Velocity Measurements of Airframe Effects on a Rotor in Low-Speed Forward Flight," *Journal of Aircraft*, Vol. 26, No. 4, 1989, p. 340.

[15]Nsi Mba, M., Favier, D., Maresca, C., and Crespi, P., "Helicopter Rotor Wake Investigation Using a Laser Doppler Anemom-

etry Technique," Computational Fluid Dynamics Conf., Lisbon, Portugal, July 1988.

[16]Cheeseman, I. C., and Haddow, C., "An Experimental Investigation of the Downwash Beneath a Lifting Rotor and Low Advance Ratios," *Vertica*, Vol. 13, No. 4, 1989, pp. 421–445.

[17]Leishman, J. G., and Bi, Nai-pei, "Measurements of a Rotor Flowfield and the Effects on a Fuselage in Forward Flight," *Vertica*, Vol. 14, No. 3, 1990, pp. 401–415.

[18]Chen, L. C., and McCroskey, J. W., "Numerical Simulation of Helicopter Multi-Bladed Rotor Flow," AIAA 26th Aerospace Sciences Meeting, AIAA Paper 88-0046, Reno, NV, 1988.

[19]Caradonna, F. X., Laub, G. H., and Tung, C., "An Experimental Investigation of the Parallel Blade-Vortex Interaction," NASA TM-86005, Nov. 1984.

[20]Berry, D. J., "A Multi-Element Vortex Lattice Method for Calculating the Geometry and Effects of a Helicopter Rotor Wake in Forward Flight," AIAA 26th Aerospace Sciences Meeting, AIAA Paper 88-0664, Reno, NV, 1988.

[21]Light, S. J., Frerking, A. A., and Norman. R. T., "Application of the Wide-Field Shadowgraph to Helicopters in Forward Flight," *Proceedings of the 46th Annual Forum of the American Helicopter Society*, Washington, DC, May 21–23, 1990, p. 1207.

[22]Tangler, J. L., "Schlieren and Noise Studies of Rotors in Forward Flight," *Proceedings of the 33th Annual Forum of the American Helicopter Society*, Washington, DC, May 1977, p. 33.5.1.

[23]Jenks, M., Dadone, L., and Gad-el-Hak, M., "Towing Tank Visualization Test of a Scale Model H-34 Rotor," *Proceedings of the 43rd Annual Forum of the American Helicopter Society*, St. Louis, MO, May 18–20, 1987, p. 825.

[24]Lehman, A. F., "Model Studies of Helicopter Rotor Flow Patterns in a Water Tunnel," *Proceedings of the 24th Annual Forum of the American Helicopter Society*, May 1968, p. 1.

[25]Leighty, B. D., Rhodes, D. B., Franke, J. M., and Jones, S. B., "A Synchronous Strobed Laser Light Sheet for Rotor Flow Visualizations," NASA TN-4266, May 1991.

[26]Briassulis, G., "Wake Structure of a Helicopter Rotor in Forward Flight," M.S. Thesis, City College of New York, New York, 1990.

[27]Yavuzkurt, R. J., Moffat, R. J., and Kays, W. M., "Full Coverage Film Cooling: 3-Dimensional Measurements of Turbulence Structure and Prediction of Recovery Region Hydrodynamics," Stanford Univ., Rept. HMT-27, Stanford, CA, 1977.

[28]Andreopoulos, J., "Statistical Error Analysis Associated with Probe Geometry and Turbulence Intensity in Hot-Wire Anemometry," *J. Phys. E: Sci. Instr.*, Vol. 16, 1983, p. 1264.

[29]Larin, A., "Vortex Wake Behind a Helicopter," *Aviatsiya i Kosmonavtika* (translated from Russian), No. 3, 1973, p. 32.

[30]Andreopoulos, J., "Improvements of the Performance of Triple Hot-Wire Probes," *Review of Scientific Instruments*, Vol. 54, No. 6, 1983, p. 733.

[31]Jorgensen, F. E., DISA-Information Rept., No. 11, 1971.

[32]Lekakis, I. C., Adrian, R. J., and Jones, B. G., "Measurement of Velocity Vectors with Orthogonal and Non-Orthogonal Triple-Sensor Probes," *Experiments in Fluids*, Vol. 7, 1989, pp. 228–240.

[33]Döbbeling, K., Lenze, B., and Leuckel, W., "Computer Aided Calibration and Measurements with Quadruple Hot-Wire Probe," *Experiments in Fluids*, Vol. 8, 1990, pp. 257–262.